# Achiral Magnetic Photonic Antenna as a Tunable Nanosource of Chiral Light

Lingfei Cui, Xingyu Yang, Benoît Reynier, Catherine Schwob, Sébastien Bidault, Bruno Gallas, Mathieu Mivelle

# An achiral magnetic photonic antenna as a tunable nanosource of chiral light

Lingfei Cui[1 #], Xingyu Yang[1 #], Benoît Reynier[1], Catherine Schwob[1], Sébastien Bidault[2], Bruno Gallas[1, *] and Mathieu Mivelle[1, *]

[1]Sorbonne Université, CNRS, Institut des NanoSciences de Paris, INSP, F-75005 Paris, France

[2]Institut Langevin, ESPCI Paris, Université PSL, CNRS, F-75005 Paris, France

*Corresponding authors:

bruno.gallas@insp.jussieu.fr

mathieu.mivelle@sorbonne-universite.fr

[#] Equally contributing authors

ORCID: 0000-0002-0648-7134

**Abstract**

Sensitivity to molecular chirality is crucial for many fields, from biology and chemistry to the pharmaceutical industry. By generating superchiral light, nanophotonics has brought innovative solutions to reduce the detection volume and increase sensitivity at the cost of a non-selectivity of light chirality or a strong contribution to the background. Here, we theoretically propose a simple achiral plasmonic resonator, based on a rectangular nanoslit in a thin metallic layer behaving as a magnetic dipole, to generate a tunable nanosource of purely chiral light working from the UV to the infrared. This nanosource is free of any background, and the sign of its chirality is externally tunable in wavelength and polarization. These unique properties, resulting from the coupling between the incident wave and the magnetic dipolar character of our nano-antenna, coupled with a method of Fluorescent Detected Circular Dichroism (FDCD), shown to be two orders of

magnitude more sensitive than classical circular dichroism measurements, thus provide a platform with deep subwavelength detection volumes for chiral molecules and a roadmap for optimizing the signal-to-noise ratios in circular dichroism measurements to reach single-molecule sensitivity.

Keywords : Magnetic dipole nano-antenna, superchiral light, plasmonics, nanophotonics, achiral nanostructures

# INTRODUCTION

Molecular chirality, the lack of superposition under mirror reflection, is of significant importance in biological systems as well as in biological and chemical processes. For instance, biological taste and smell receptors are sensitive to enantiomers, the two reflected images of a chiral molecule, and can differentiate them chemically by producing different responses that we interpret, for example, as radically different smells.[1] This asymmetry is essential in the case of physiological drug action, where, in the worst case, one enantiomer acts as a drug while the other has harmful effects.[2] Chiral molecules reveal their chirality through interaction with another chiral entity, such as circularly polarized light. Circular dichroism (CD) spectroscopy exploits the difference in light absorption for right and left circular polarizations to detect and identify chiral molecules. This is why intense research based on optical nanostructures has been developed for several years, aiming at reducing the detection volume while increasing the sensitivity. This research is based on the concept of superchiral light, defined as a chirality density higher than propagative circularly polarized light.[3] Indeed, the CD is proportional to the chirality density $C = -\frac{\varepsilon_0 \omega}{2} Im(\boldsymbol{E}^*.\boldsymbol{B})$, where $\varepsilon_0$ and $\omega$ are the permittivity of vacuum and the angular frequency, respectively, and **E** and **B** are the time dependent electric and

magnetic fields.[4-6] Although the interaction between a chiral medium and an optical nanostructure is a complex mechanism,[7-10] the ability of resonant optical nanostructures, such as photonic nano-antennas, to enhance the electric and magnetic optical near-fields allows the optimization of C, and thus of the CD and FDCD signals of molecules in their vicinity, increasing the sensitivity in enantioselectivity while decreasing the interaction volume.

So far, the generation of superchiral fields has mainly relied on chiral plasmonic resonators or chiral 3D architectures.[11-27] In these approaches, the difficulty lies in the external control of the sign of the chirality density which is fixed by the shape of the resonators. Recently, other interesting approaches using achiral plasmonic[8, 11, 28-30] or dielectric[9, 31-34] resonators featuring chiral near-fields yielding some signatures of CD have been proposed. But while achiral resonators hold the exciting property to control the average sign of C by either changing the angle of illumination[35] or polarization[36-39] of the incoming light, this effect is obtained at the cost of a non-uniform distribution of the chirality density around the photonic nanostructure, diminishing the overall enhancement of C and reducing the experimental interest of these types of achiral nano-antennas. Here, we theoretically and numerically propose to generate a pure and nanoscale hot spot of chiral light in the near-field by using a single achiral plasmonic nano-resonator behaving, in agreement with Babinet principle,[40-43] as a magnetic dipole and based on a rectangular nanoslit (NS).[44-46] When observed in transmission, this hot-spot of chiral light, generated by a linearly polarized excitation, is free of any background from the excitation beam and its sign can be tuned by either changing the wavelength or the polarization angle of the incoming light. Moreover, we demonstrate the distinct advantage of using a NS over other achiral plasmonic antennas used so far, based on nano-rod (NR) geometries, in terms of yielding uniform superchiral light. Finally, to fully understand the physical mechanisms underlying these unique properties, we demonstrate, via an

analytical model, that these effects are due to the magnetic dipolar nature of our NS which constructively interferes with the incident optical excitation. The resulting nanovolume of superchiral light can then serve as a nanosource to excite chiral molecules in solution present only in the nanoslit. Therefore, detecting the fluorescence or autofluorescence of the molecules present in this chiral hotspot, particularly the difference in emission between a right chiral and a left chiral excitation, makes it possible to measure the CD for a small number of molecules.[47] Indeed the sensitivity of detectors reaches the single photon limit and plasmonic nano-apertures are particularly well suited to detect single molecules in solution.[48] Thus, the nanoplatform we propose here to generate a nanosource of tunable superchiral light, free of background noise, provides a roadmap for optimizing signal-to-noise ratios in emission-based rather than absorption-based circular dichroism measurements in order to achieve single molecule sensitivity (see the Supporting Information for the description of this approach in FDCD).

# RESULTS AND DISCUSSION

The rectangular NS used in this study is schematically represented in **Figure 1**a (see Supporting Information for simulation details). It is made in a thin gold layer of thickness H=40 nm deposited on a glass substrate. The width W of the NS is fixed at 20 nm and its length L varies from 50 to 90 nm in steps of 10 nm. The excitation is performed from the glass substrate by a linearly polarized plane wave, with a polarization angle θ, and propagates along the positive Z axis (**Figure 1**a). θ was chosen with respect to the short axis of the NS, light polarized at $\theta = 0^{\circ}$ being along the X axis of the NS (**Figure 1**b). In this paper, we mainly observe the distribution of electromagnetic fields in a plane within the rectangular NS (XY plane when Z=20 nm) and for two points, point A is the geometric

center (0,0) of the NS and point B is 5 nm away from the short edge and on the y axis. These two points correspond to the positions of the maximum electric and magnetic fields in the NS, respectively. In the FDTD calculations, the mesh size is set at 1 nm to ensure an accurate optical response of the NS. **Figures 1**c and **1**d show the spectral responses of the NS for different lengths L. These spectra represent the enhancement of the electric (**Figure 1**c) and magnetic (**Figure 1**d) fields normalized to the incident wave, in the center (point A) and side (point B) of the NS, 20 nm above the glass substrate and for $\theta = 45°$, respectively. We observe resonant behaviours of the electric and magnetic fields with a linear red shift when the length of the NS increases. In the following, we will focus on an NS length of 80 nm, yielding a resonance at 680 nm.

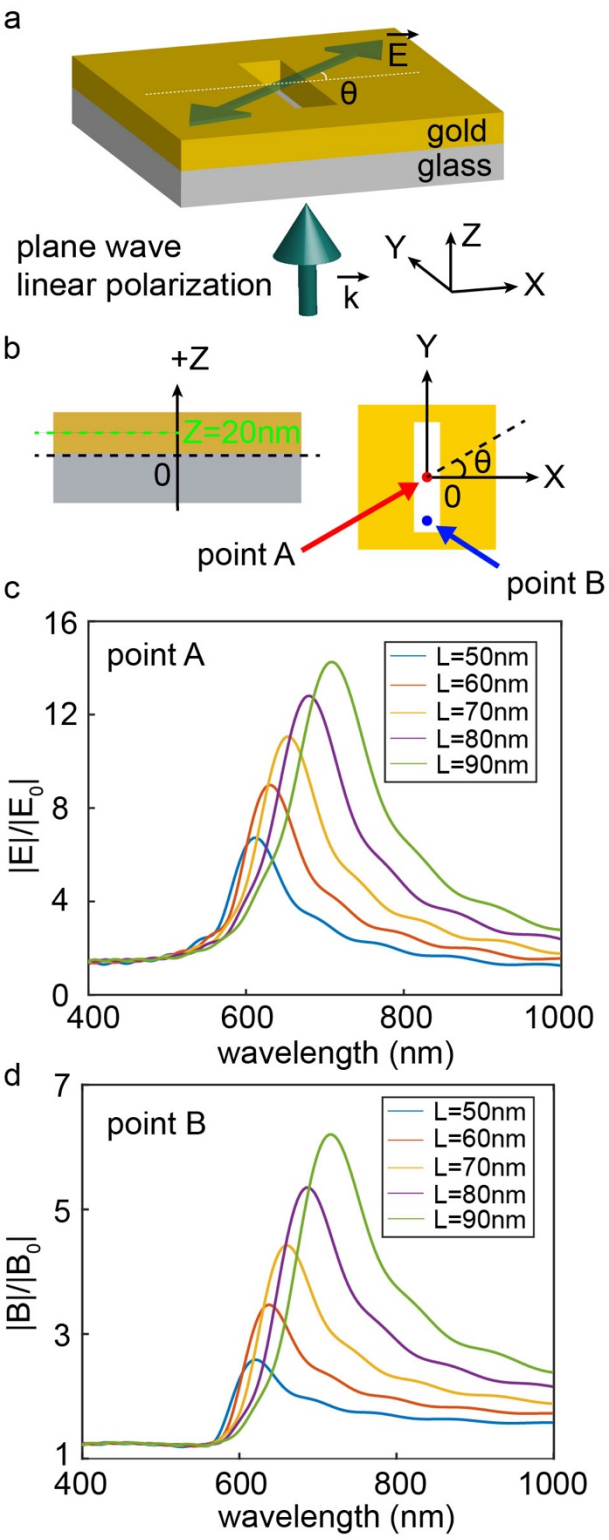


**Figure 1**. *Schematic representations and spectral responses of the magnetic dipolar NS. a) 3D and b) 2D representation of the rectangular NS in a thin gold layer of 40 nm. The vector **k** represents the direction of propagation of the linearly polarized incident plane wave, and θ, the angle of this polarization with respect to the NS's transverse axis (Ox).*

*c) Electric and d) magnetic spectral responses for different lengths of the optical NS shown in a) and b), for a width of 20 nm and θ = 45°. The spectra represent the electric and magnetic fields normalized by the incident wave, respectively, at points A (geometric center of the NS in the three dimensions of space) and B (at the center of the NS in XZ and 5 nm from the edge of the NS in Y), as shown in the inset in b).*

In order to describe the electromagnetic behavior of this NS further, **Figures 2**a and **2**b provide the spatial distributions of the electric and magnetic field enhancements in the observation plane of the NS, and excited for θ=45° at the wavelength λ=680 nm. We see, in good agreement with Babinet's principle, that the distribution of the electric and magnetic fields are opposite with respect to an electric dipole antenna such as a plasmonic NR[42, 43]. In particular, the **E**-field is concentrated homogeneously in the center of the NS while the **B**-field is maximum at the edges. Also, these electric and magnetic fields are increased by a factor of about 13 and 6 with respect to the incoming light, respectively. Furthermore, **Figures 2**c and **2**d display the time-average electric and magnetic energy density $U_e = \frac{\varepsilon_0}{4}|\boldsymbol{E}|^2$ and $U_b = \frac{|\boldsymbol{B}|^2}{2\mu_0}$, where $\mu_0$ is the permeability of vacuum, at the points A and point B of the NS as a function of the wavelength of the incoming plane wave and of the angle of its linear polarization with respect to the NS. We see that $U_e$ and $U_b$ are maximum at λ = 680 nm for a polarization angle of θ = 0° corresponding to a polarization along the short axis of the NS, in good agreement with experiments demonstrating higher transmission for that polarization[44, 46]. These observations support the hypothesis of a magnetic dipole character for the NS[45, 46]. It is important to notice that the electric and magnetic energy densities are the same inside the NS for opposite angles ±θ.

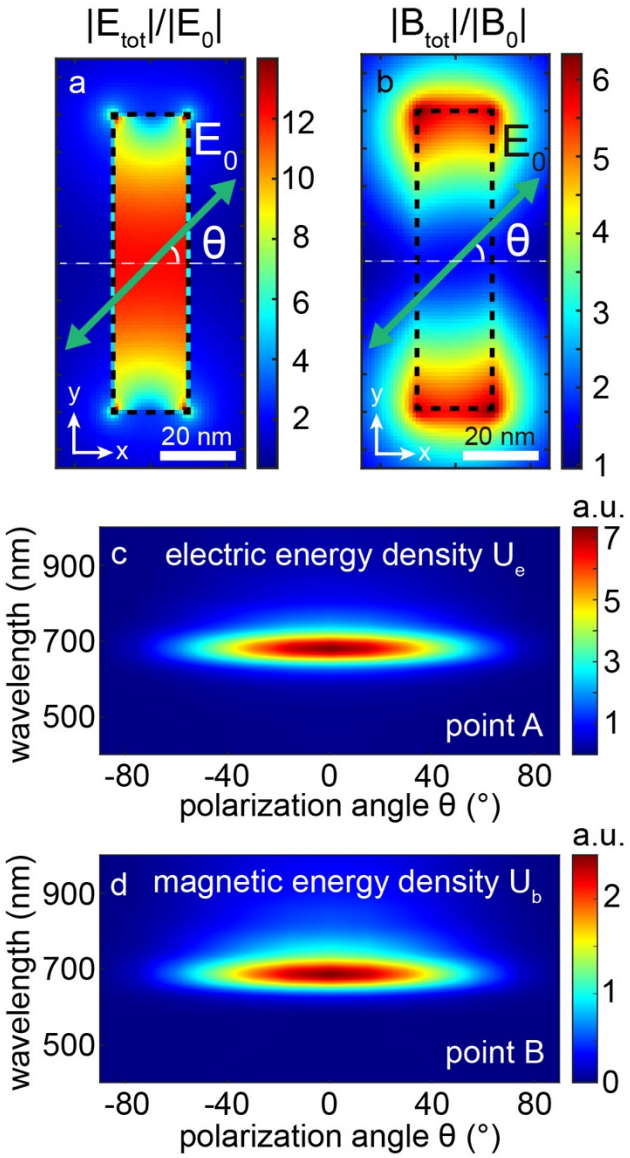


**Figure 2**. *Electromagnetic field distribution and spectral energy responses. Spatial distribution of a) electric and b) magnetic fields in an XY plane at the center of the NS in Z, at lambda=680 nm, and for a polarization angle θ = 45° (See SI for electric and magnetic distributions under different angles θ). The dashed lines represent the edges of the NS. Spectral responses of c) the electric and d) the magnetic energy densities as a function of the incident polarization angle θ and wavelength respectively at points A and B (inset of **Figure 1**b).*

From the electromagnetic fields calculated and displayed in **Figures 2**a and **2**b, we have computed the chirality density enhancement $C_{enh}$ in the NS, defined as $C/|C_{cpl}|$, with $C_{cpl}$ the chirality density of a circularly polarized light, without the aperture, carrying the same

power as the linearly polarized excitation impinging on the NS. **Figure 3**a presents $C_{enh}$ at the geometric center point A of the NS as a function of the wavelength for two polarization angles (45° and -45°). The results are striking. Indeed, as we can see, for opposite polarization angles $\theta=\pm45^{\circ}$, the sign of chirality density is reversed, something that is true for any pairs of opposite angle θ but with a lower magnitude of $C_{enh}$ (see Supporting Information). Also, and surprisingly, the sign of the chirality density is changed when crossing the resonant frequency of 680 nm, $C_{enh}$ being close to 0 at the resonance. Two opposite extrema are then observed on each side of the resonance, one at 645 nm and the other at 718 nm, with chirality density enhancements of respectively 4.5 and 3.5, in absolute value. These values of the chirality density within the nanoslit thus become larger than the one observed for a circularly polarized plane wave thanks to the near-field enhancement of the electric and magnetic fields observed in **Figure 2**. From these results, the spatial distributions of the chirality density in the observation plane and for the wavelengths of 645, 680 and 718 nm are shown in **Figure 3**b and **3**c, for θ = +45° and θ = -45°, respectively. Remarkably, while the local chirality density distributions around plasmonic antennas have always been observed as non-uniform[36, 38, 39], in this case, they are perfectly homogeneous at the wavelengths of the two extrema (645 and 718 nm). Also, as we can see in **Figures 3**b and **3**c, the sign of the chirality density changes altogether by switching the polarization from +45° to -45°. Therefore, the NS provides a pure nanosource of chiral light tunable using either the incoming wavelength or polarization and free of any background (see **Figure s2** for transmission enhancement), something that no other system can currently achieve. Furthermore, the chirality distribution averages 0 within the NS at the resonance wavelength for a linearly polarized excitation. However, it reaches a maximum at resonance for a circularly polarized excitation, and the sign of C can be changed depending on the helicity of the light (see **Figure s3**). Although C is stronger in the case of circular polarization, we have

chosen in this manuscript to focus on the coupling between this achiral nanoslit with achiral linear polarization. Nevertheless, all the optical properties of nano-apertures demonstrate the versatility of this nano-object for its use in CD experiments. Therefore, depending on the excitation polarization of this NS, the chirality density can be fully controlled and enhanced at the nanoscale over a wide spectral range. Indeed, when measuring circular dichroism experimentally, photoelastic modulators are used to modulate the incident light polarization on chiral molecules, and they produce all possible polarizations, from linear (+45 and -45°) to right and left circular. Therefore, by demodulating the signal, the NS gives access to a very large spectral range covering about 300 nm, centered on the resonance wavelength, and whose sign of the chirality density can be fully controlled over this range. Moreover, by changing the NS's length or material, the whole visible spectrum can be covered, as well as the ultraviolet where chiral biomolecules efficiently absorb light[49] (see **Figure S4, s16 and s17**). Also, fabrication defects of the NS, such as rounded corners, would only marginally affect the optical and chiral response of the nanostructure (see **Figure s5**). Finally, and remarkably, placing this type of plasmonic nanostructure in a lattice does not change the chirality density distribution in the NS nor its tunability, thus facilitating the use of NSs experimentally (See **Figure s**7). Note that defects in the nanofabrication or granularity of the gold layer could lead to an intrinsic chirality signal. One way to avoid this would be to use single crystal gold flakes and to nanofabricate these antennas by high aspect ratio lithography techniques such as a Helium focused ion beam. Also, using these antennas in an array would average these defects over a large number of nanoslits. Finally, a characterization of the CD of these magnetic antennas without the presence of chiral molecules would allow a quantitative calibration of the chiral behavior of bare antennas.

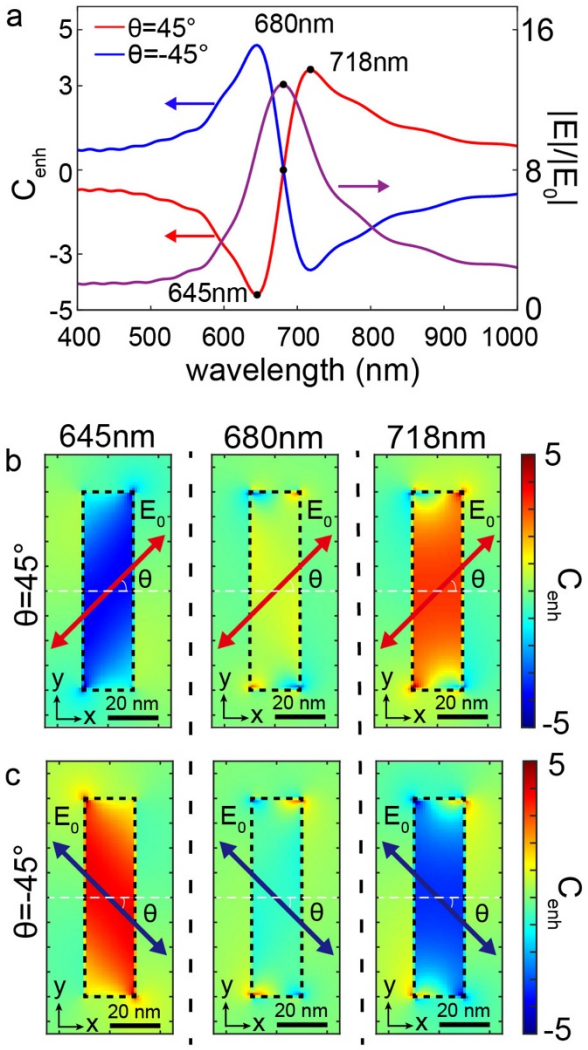


**Figure 3**. *Spectral and spatial responses of the chirality density. a) Spectral responses in chirality density (blue and red lines) and intensity (purple line) for a NS of length 80 nm, width 20 nm, for two opposite angles θ = ±45° and at point A (inset of* ***Figure 1****b). Spatial distribution of the chirality density in an XY plane within the NS in Z, for three characteristic wavelengths and for b) θ = +45° and c) θ = -45°.*

To further investigate these findings, and to compare the results of our magnetic dipole antenna with its electric counterpart, the volumetric chirality density $C_{vol}$ generated by the NS is compared to that of a gold NR, having the dimensions W=20 nm, H=40 nm and L=70 nm, and creating a $C_{enh}$ maximum at $\lambda$ = 645 nm (see Supporting Information). For this purpose, we simulated the electromagnetic response of both types of antennas (NS

and NR) supported by glass and excited by a plane wave propagating along the positive Z-axis from the substrate. The wavelength was set to 645 nm and the incident field was linearly polarized with an angle θ with respect to the short axis of the NS and NR (**Figures 4**a and **4**b). For this study, we consider how such antennas could be exploited experimentally to study chiral molecules. Thus, in the case of the NS, only the internal volume of the NS is considered useful in terms of near-field light-matter interactions, and this volume is equal to 64000 $nm^3$. On the other hand, only the part surrounding the NR would be accessible to potential chiral molecules, which, for a similar volume, corresponds to a thickness, of 6 nm around the NR (64704 $nm^3$, when neglecting the plane on which the NR sits on the glass substrate). **Figure 4**c plots $C_{vol}$ for the NS and NR as a function of the angle θ. Several observations can be made. First, we see that for the same angle, the volumetric chirality densities have opposite signs. Second, in absolute value, the NS featured $C_{vol}$ values that are increased by a factor of 9 compared to the NR, for all polarization angles. This is due to the non-uniformity of the chirality density around the NR which decreases the volumetric average $C_{vol}$, in contrast to the NS which generates a pure chiral light as illustrated by the insets of **Figure 4**c. In the insets of **Figure 4**c, the chirality density distributions were calculated in middle plane of the NS and 5 nm above the NR. Finally, the comparative advantage of the NS is not limited to the increase of the chirality density in the near field but must also be highlighted with respect to the interaction volume that a far field excitation generates. Indeed, while the chiral signal provided by the NS would be free of any background signal due to the opacity of the gold layer in the case of transmission measurements, the one generated by the NR would be added to background chiral light-matter interactions occurring during the propagation of the incoming plane wave far from the antenna. This is something that is not considered here, but which must be taken into account if one wants to use such achiral antennas experimentally.

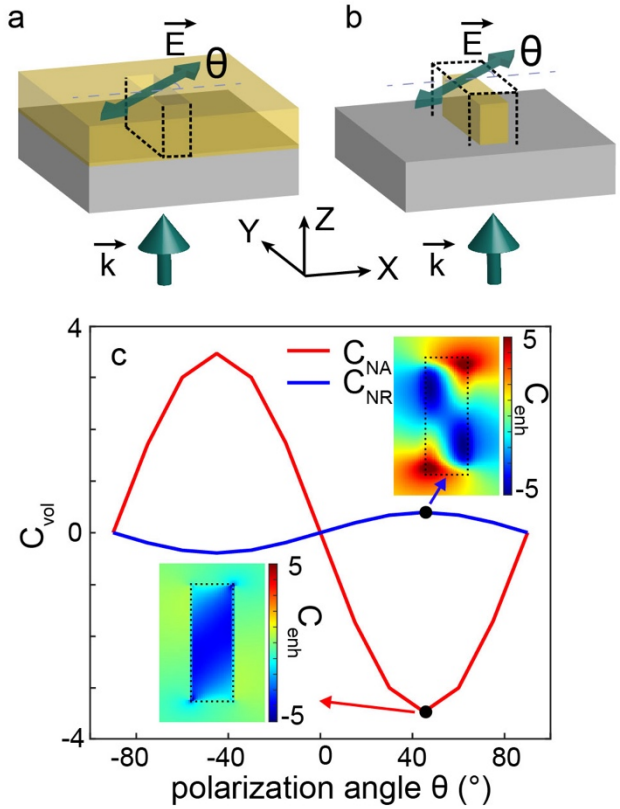


**Figure 4**. *Comparison of gold NS versus NR. Schematic representations of a) the NS and b) the NR, excited by a plane wave linearly polarized by an angle θ with respect to the transverse axis of the antennas (Ox). The dotted lines determine the volume considered in the calculation of $C_{vol.}$ c)Volumetric chirality density inside the NS and in the near field of the NR for different angles θ of the linear polarization of the excitation light. In the insets are represented the spatial distributions of the chirality density around these two antennas for θ = +45°, demonstrating the inhomogeneity of C in the case of the plasmonic NR.*

## Point-like dipole model

The wavelength and polarization tunability as well as the nanoscale homogeneity of the chirality density that our NS allows is very different from what was observed in the past in chiral[50] or achiral plasmonic nanostructures[51] such as for plasmonic NRs[36, 38, 39, 52]. The unusual properties demonstrated in this work are intrinsically linked to the magnetic dipolar character of the NS[46]. In particular, the interaction between the incident light and

the magnetic dipole emission of the antenna is at the origin of these unique characteristics. In order to highlight this coupling, we use a point-like dipole model, similarly to what was carried out for the study of electric dipolar antennas [36].

The total fields radiated by a point-like magnetic dipole with moment **m**, containing both near-field and far-field contributions and decomposed in a magnetic field $\mathbf{B}_{rad}$ and an electric field $\mathbf{E}_{rad}$ contributions observed in the direction **n** at a distance r from the position of the dipole, are given by:[40]

$$\boldsymbol{B}_{rad} = \frac{1}{4\pi\mu_o}\left\{k^2(\boldsymbol{n}\times\boldsymbol{m})\times\boldsymbol{n}\frac{e^{ikr}}{r} + [3\boldsymbol{n}(\boldsymbol{n}.\boldsymbol{m}) - \boldsymbol{m}]\left(\frac{1}{r^3} - \frac{ik}{r^2}\right)e^{ikr}\right\} \quad (2a)$$

$$\boldsymbol{E}_{rad} = -\frac{Z_o}{4\pi}k^2(\boldsymbol{n}\times\boldsymbol{m})\frac{e^{ikr}}{r}\left(1 - \frac{1}{ikr}\right) \quad (2b)$$

with k the wavevector, $Z_o$ the impedance of vacuum and $\mu_o$ the permeability of vacuum. The amplitude of the magnetic moment is given by $\boldsymbol{m} = \alpha^{mm}\boldsymbol{H}_o$ with $\alpha^{mm}$ the magnetic polarizability tensor and $\mathbf{H}_o$ the incident magnetic field (see Supporting Information). Interestingly, we see that $\mathbf{E}_{rad}$ and $\mathbf{B}_{rad}$ are always orthogonal; therefore, the chirality density $C_{rad} = -\epsilon_o\omega\mathrm{Im}(\mathbf{E}_{rad}^*.\mathbf{B}_{rad})/2$, corresponding to the chirality density calculated from the radiative fields only, is always equal to zero in the near-field. However, the magnetic field contains a longitudinal component in the near-field that generates an elliptically polarized component that is characterized by a transverse spin angular momentum non vanishing in the near-field (non-zero spin density), as already pointed out for electric point-like dipoles.[53] This is remarkable, since in the far field, the chirality density and spin density are related and linked the same quantity which is the helicity of the propagating light. But, in the near field, due to the evanescent character of the electric and magnetic fields these two quantities are no longer proportional.[5] For a point-like dipole to generate a non-vanishing chirality density, it is required to take into account the

contribution of the incident $\mathbf{E}_o$ and $\mathbf{B}_o$ fields as well as the radiated $\mathbf{E}_{rad}$ and $\mathbf{B}_{rad}$ fields so that the total fields are $\mathbf{E}_{tot}=\mathbf{E}_{rad}+\mathbf{E}_o$ and $\mathbf{B}_{tot}=\mathbf{B}_{rad}+\mathbf{B}_o$. The interferences between the incident and radiated fields, in amplitude, polarization, and phase, therefore allow the generation of a non-zero chirality density. Here, the resonance of the magnetic dipole moment is described with a lorentzian spectral dependence, with a phase shift that reaches $\pi/2$ when the dipole is driven at resonance. The magnetic dipole, oriented along x, is then excited by the magnetic field of a linearly polarized plane wave, propagating along z and polarized at 45° with respect to the orientation of the magnetic dipole. Taking into account that in the near field k.r << 1, the expression of the chirality density can then be simplified to the first order in k.r. Considering that in the case of the NS the field enhancement $\xi = \mathbf{E}_{tot}/\mathbf{E}_o$=13 (**Figures 1**c and **2**a), the expression of C taking into account the total fields becomes $C_{tot} = -\varepsilon_o \omega Im\left((\boldsymbol{E}_0 + (\xi - 1)\boldsymbol{E}_{rad})^*.(\boldsymbol{B}_0 + \boldsymbol{B}_{rad})\right)/2$ (derivation detailed in SI 3) which yields :

$$C_{tot}(\pm 45°) = \pm \frac{\omega}{8 Z_o c^2 r^3}\left(\xi k.r.\alpha' - \alpha''\right) + 0\left(k.r^2\right) \qquad (2)$$

where $\alpha'$ and $\alpha''$ are the real and imaginary parts of the magnetic polarizability, respectively.

**Figure 5** shows the spectral dependence of $C_{tot}$ derived from equation 2, 20 nm above the dipole in z and for both polarization angles +/-45°. The results observed for the normalized chirality density of the point-dipole model in **Figure 5**a are in excellent agreement with the spectral responses of the enhanced chirality density $C_{enh}$ within the NS in **Figure 3**a. An inversion of the sign of the chirality density is found at the resonance of the magnetic dipole, with two spectral extrema on each side of the resonance wavelength. Also, the sign of the chirality density changes with the angle of the polarization of the plane wave incident on the dipole. These observations are perfectly

explained by Equation (5) in SI due to the sin(θ) term. This inversion can also be explained by the excitation of the nanoslit's two longitudinal and transverse modes. The fact that these two modes resonate at different wavelengths implies that the phase shift across these resonances will occur at different frequencies, generating a non-zero chirality density inside the nanoslit. Moreover, depending on the angle of linear polarization (+ or - 45°) or the ellipticity of circular polarization (right or left), the phase shift between the two modes will be of opposite sign. This phenomenon generates an inversion of the chirality density in the antenna as a function of angle or ellipticity (see Figure s14). Furthermore, the spectral dependence is directly related to the large field enhancement factor which allows the real part of the magnetic dipole moment to dominate the spectral variations of $C_{tot}$. One can expect the spectral variations of $C_{tot}$ to be dominated by the imaginary part of the magnetic dipole moment for smaller electric field enhancements (see Supporting Information SI.3).

Using the expression of $C_{tot}$ (Equation (2)), the chirality density distributions in an xy plane 20 nm away from the dipole were calculated and are shown in **Figures 5**b and **5**c. We used an incident polarization of 45° and -45°, a field enhancement ξ = 13 and wavelengths of 645 nm, 680 nm and 718 nm.

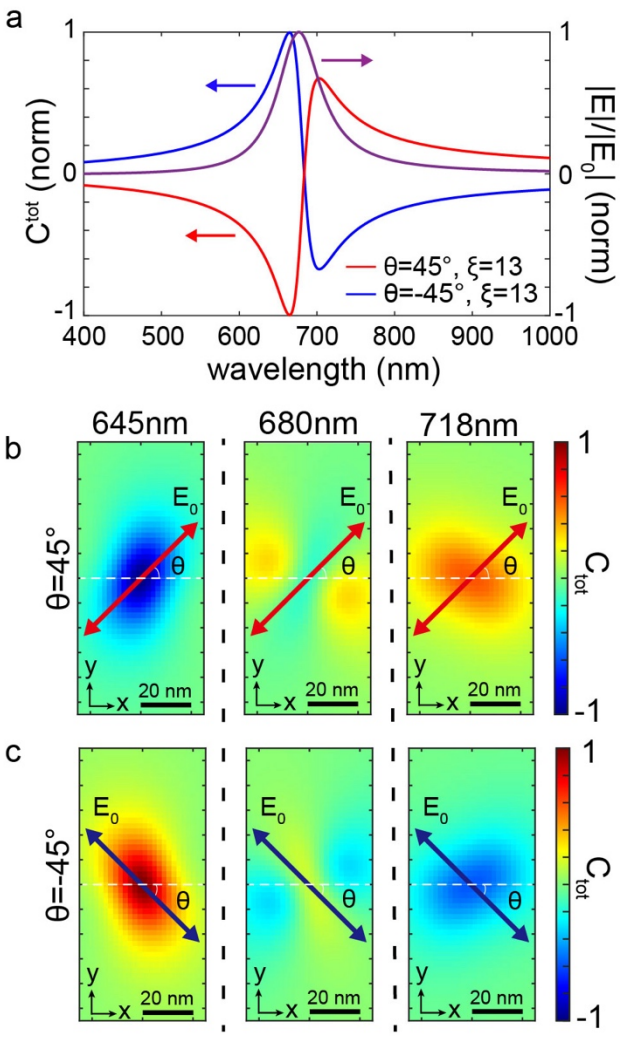


**Figure 5.** *Spectral and spatial chirality density responses obtained using a magnetic dipole model. (a) Spectral chirality density and intensity responses 20 nm above a magnetic dipole interacting with a linearly polarized plane wave propagating along the positive Z axis and having a polarization angle relative to the dipole of θ = ±45°. Spatial distribution of the chirality density in an XY plane, 20 nm above the magnetic dipole, for the three characteristic wavelengths corresponding to the extrema and the resonance and for (b) θ = +45° and (c) θ = -45°.*

Once again, we see a perfect agreement between the numerical results obtained for the NS simulations (**Figures 3**b and **3**c) and for the analytical approach using a dipole model

(**Figures 5**b and **5**c). In particular, a uniform chirality density distribution is obtained for each extremum ($\lambda$ = 645 nm and 718 nm). At resonance ($\lambda$ = 680 nm), the chirality density is no longer uniform, much smaller and vanishes on the average exactly like for the numerical results of the NS at resonance. These observations are very different from those made for NRs where the field enhancement was not taken into account.[36, 38, 39] These observations offer a new roadmap in the design of nanostructures featuring enhanced chirality densities controlled externally by linearly polarized light and wavelengths, in particular through the optimization of magnetic dipolar resonances.

As a final remark, it is important to note that, as recently reported,[10] the increase of the CD of a chiral material in the presence of an optical nanostructure is multifactorial and is not only related to the chirality density. To investigate whether the increase of the chirality density in the nanoslit provides a significant gain in CD compared to a far field excitation of a chiral material, we performed a series of simulations with a chiral material embedded in the nanoslit. By comparing the simulated CD signal with the NS and without it, we observe an increase of the CD by about one order of magnitude in our magnetic dipole antenna over its entire spectral response (Figure s11), in good agreement with the increase in chirality density within the nanoslit.

# CONCLUSIONS

In conclusion, we have demonstrated numerically and theoretically that the coupling between an achiral linearly polarized propagating wave and a magnetic dipolar achiral photonic NS produces a nanosource of purely superchiral light free of any background. Furthermore, we have demonstrated that the sign of the created chirality density was externally tunable simply by changing the excitation wavelength or the angle of the linear polarization incident on the structure. Finally, we have demonstrated that the useful

chirality density produced by this photonic NS exceeded by one order of magnitude that of other types of achiral nanotructures such as gold NRs behaving as electric dipoles, highlighting the contribution of the magnetic dipole in the case of the nanoslit. By creating externally and on-demand tunable and background-free superchiral light nanosources, this work opens unique perspectives for the ultrasensitive detection of chiral molecules in solution at the nanoscale, with exciting perspectives to reach single-molecule sensitivity by monitoring, for instance, chiral luminescence instead of absorption.

## Supporting Information

The Supporting Information is available free of charge

Additional information about the increase of chirality density in a nanoslit (NS) as a function of angle and wavelength, the transmission enhancement through the NS, the chirality density under circular polarization excitation, the spectral responses in volumetric chirality density for NSes of different lengths made in a gold layer and aluminum, the spectral responses in volumetric chirality density for two types of NS, one with 90° angled corners and the other with rounded corners, the chirality density enhancement study for a nanorod, the spectral response in volumetric chirality density for an NSes array, the derivation of the point-like dipole model, the simulation parameters, the CD enhancement of a chiral material in the nanoslit.

## Funding Sources

We acknowledge the financial support from the Agence national de la Recherche (ANR-20-CE09-0031-01, ANR-18-CE09-0010), from the Institut de Physique du CNRS (Tremplin@INP 2020). Two of the authors (L.C. and X.Y.) acknowledge the support of the China Scholarship Council.

## Conflict of Interest

The authors declare no conflict of interest.

## Associated Content

Lingfei Cui; Xingyu Yang; Benoît Reynier; Catherine Schwob; Sébastien Bidault; Bruno Gallas; Mathieu Mivelle. An achiral magnetic photonic antenna as a tunable nanosource of superchiral light. Arxiv. https://arxiv.org/abs/2301.11044 (accessed January 26, 2023).

## Table of content graphic

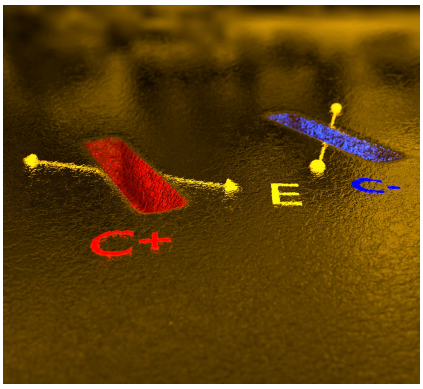

# References


1. Laska, M.; Teubner, P., Olfactory discrimination ability of human subjects for ten pairs of enantiomers. *Chemical senses* **1999,** *24* (2), 161-170.
2. Davies, N. M.; Teng, X. W., Importance of chirality in drug therapy and pharmacy practice: Implications for psychiatry. *Advances in Pharmacy* **2003,** *1* (3), 242-252.
3. Tang, Y.; Cohen, A. E., Optical chirality and its interaction with matter. *Phys. Rev. Lett.* **2010,** *104* (16), 163901.
4. Lipkin, D. M., Existence of a new conservation law in electromagnetic theory. *Journal of Mathematical Physics* **1964,** *5* (5), 696-700.
5. Bliokh, K. Y.; Nori, F., Characterizing optical chirality. *Phys. Rev. A* **2011,** *83* (2), 021803.
6. Coles, M. M.; Andrews, D. L., Chirality and angular momentum in optical radiation. *Phys. Rev. A* **2012,** *85* (6), 063810.
7. Poulikakos, L. V.; Gutsche, P.; McPeak, K. M.; Burger, S.; Niegemann, J.; Hafner, C.; Norris, D. J., Optical chirality flux as a useful far-field probe of chiral near fields. *ACS photonics* **2016,** *3* (9), 1619-1625.
8. Lee, S.; Yoo, S.; Park, Q.-H., Microscopic origin of surface-enhanced circular dichroism. *ACS Photonics* **2017,** *4* (8), 2047-2052.
9. Raziman, T.; Godiksen, R. H.; Muller, M. A.; Curto, A. G., Conditions for enhancing chiral nanophotonics near achiral nanoparticles. *ACS Photonics* **2019,** *6* (10), 2583-2589.
10. Both, S.; Schäferling, M.; Sterl, F.; Muljarov, E. A.; Giessen, H.; Weiss, T., Nanophotonic chiral sensing: how does it actually work? *ACS Nano* **2022,** *16* (2), 2822-2832.
11. Govorov, A. O.; Fan, Z.; Hernandez, P.; Slocik, J. M.; Naik, R. R., Theory of circular dichroism of nanomaterials comprising chiral molecules and nanocrystals: plasmon enhancement, dipole interactions, and dielectric effects. *Nano. Lett.* **2010,** *10* (4), 1374-1382.
12. Abdulrahman, N. A.; Fan, Z.; Tonooka, T.; Kelly, S. M.; Gadegaard, N.; Hendry, E.; Govorov, A. O.; Kadodwala, M., Induced chirality through electromagnetic coupling between chiral molecular layers and plasmonic nanostructures. *Nano. Lett.* **2012,** *12* (2), 977-983.
13. Hendry, E.; Mikhaylovskiy, R.; Barron, L.; Kadodwala, M.; Davis, T., Chiral electromagnetic fields generated by arrays of nanoslits. *Nano. Lett.* **2012,** *12* (7), 3640-3644.
14. Kaschke, J.; Gansel, J. K.; Wegener, M., On metamaterial circular polarizers based on metal N-helices. *Opt. Express* **2012,** *20* (23), 26012-26020.
15. Droulias, S.; Yannopapas, V., Broad-band giant circular dichroism in metamaterials of twisted chains of metallic nanoparticles. *J. Phys. Chem. C* **2013,** *117* (2), 1130-1135.
16. Yin, X.; Schäferling, M.; Metzger, B.; Giessen, H., Interpreting chiral nanophotonic spectra: the plasmonic Born–Kuhn model. *Nano. Lett.* **2013,** *13* (12), 6238-6243.

17. Zhukovsky, S. V.; Chigrin, D. N.; Kremers, C.; Lavrinenko, A. V., Dichroism, chirality, and polarization eigenstates in Babinet nanoslot-dimer membrane metamaterials. *Photonics and Nanostructures-Fundamentals and Applications* **2013,** *11* (4), 353-361.
18. Kondratov, A.; Gorkunov, M.; Darinskii, A.; Gainutdinov, R.; Rogov, O.; Ezhov, A.; Artemov, V., Extreme optical chirality of plasmonic nanohole arrays due to chiral Fano resonance. *Phys. Rev. B* **2016,** *93* (19), 195418.
19. Schäferling, M.; Engheta, N.; Giessen, H.; Weiss, T., Reducing the complexity: Enantioselective chiral near-fields by diagonal slit and mirror configuration. *ACS photonics* **2016,** *3* (6), 1076-1084.
20. Špačková, B.; Wrobel, P.; Bocková, M.; Homola, J., Optical biosensors based on plasmonic nanostructures: a review. *Proceedings of the IEEE* **2016,** *104* (12), 2380-2408.
21. Wang, Z.; Wang, Y.; Adamo, G.; Teh, B. H.; Wu, Q. Y. S.; Teng, J.; Sun, H., A novel chiral metasurface with controllable circular dichroism induced by coupling localized and propagating modes. *Advanced Optical Materials* **2016,** *4* (6), 883-888.
22. García-Guirado, J.; Svedendahl, M.; Puigdollers, J.; Quidant, R., Enantiomer-selective molecular sensing using racemic nanoplasmonic arrays. *Nano. Lett.* **2018,** *18* (10), 6279-6285.
23. Ai, B.; Luong, H. M.; Zhao, Y., Chiral nanohole arrays. *Nanoscale* **2020,** *12* (4), 2479-2491.
24. Luong, H. M.; Pham, M. T.; Nguyen, T. D.; Zhao, Y., Active Ag/Co composite chiral nanohole arrays. *J. Phys. Chem. C* **2020,** *125* (1), 716-723.
25. Petronijevic, E.; Ali, H.; Zaric, N.; Belardini, A.; Leahu, G.; Cesca, T.; Mattei, G.; Andreani, L.; Sibilia, C., Chiral effects in low-cost plasmonic arrays of elliptic nanoholes. *Optical and Quantum Electronics* **2020,** *52* (3), 1-10.
26. Qu, Y.; Bai, Y.; Aba, T.; Ullah, H.; Abudukelimu, A.; Huang, J.; Gou, T.; Li, J.; Zhang, Z., Chiral near-fields induced by plasmonic chiral conic nanoshell metallic nanostructure for sensitive biomolecule detection. *J. Phys. Chem. C* **2020,** *124* (25), 13912-13919.
27. Wu, B.; Wang, M.; Sun, Y.; Wu, F.; Shi, Z.; Wu, X., Near-infrared chirality of plasmonic metasurfaces with gold rectangular holes. *Advanced Composites and Hybrid Materials* **2022,** *5* (3), 2527-2535.
28. Slocik, J. M.; Govorov, A. O.; Naik, R. R., Plasmonic circular dichroism of peptide-functionalized gold nanoparticles. *Nano. Lett.* **2011,** *11* (2), 701-705.
29. Maoz, B. M.; Ben Moshe, A.; Vestler, D.; Bar-Elli, O.; Markovich, G., Chiroptical effects in planar achiral plasmonic oriented nanohole arrays. *Nano. Lett.* **2012,** *12* (5), 2357-2361.
30. Nesterov, M. L.; Yin, X.; Schäferling, M.; Giessen, H.; Weiss, T., The role of plasmon-generated near fields for enhanced circular dichroism spectroscopy. *Acs Photonics* **2016,** *3* (4), 578-583.
31. García-Etxarri, A.; Dionne, J. A., Surface-enhanced circular dichroism spectroscopy mediated by nonchiral nanoantennas. *Phys. Rev. B* **2013,** *87* (23), 235409.
32. Garcia-Guirado, J.; Svedendahl, M.; Puigdollers, J.; Quidant, R., Enhanced chiral sensing with dielectric nanoresonators. *Nano. Lett.* **2019,** *20* (1), 585-591.

33. Hu, J.; Lawrence, M.; Dionne, J. A., High quality factor dielectric metasurfaces for ultraviolet circular dichroism spectroscopy. *ACS Photonics* **2019,** *7* (1), 36-42.
34. Feis, J.; Beutel, D.; Köpfler, J.; Garcia-Santiago, X.; Rockstuhl, C.; Wegener, M.; Fernandez-Corbaton, I., Helicity-preserving optical cavity modes for enhanced sensing of chiral molecules. *Phys. Rev. Lett.* **2020,** *124* (3), 033201.
35. Guth, N.; Gallas, B.; Rivory, J.; Grand, J.; Ourir, A.; Guida, G.; Abdeddaim, R.; Jouvaud, C.; De Rosny, J., Optical properties of metamaterials: Influence of electric multipoles, magnetoelectric coupling, and spatial dispersion. *Phys. Rev. B* **2012,** *85* (11), 115138.
36. Schäferling, M.; Yin, X.; Giessen, H., Formation of chiral fields in a symmetric environment. *Opt. Express* **2012,** *20* (24), 26326-26336.
37. Yao, H.; Zhong, S.; Yi, H.; Cui, D.; Pan, C.-L., Handedness-switchable optical chirality in one-dimensional periodic plasmonic-grooves for circular dichroism and simultaneous refractive index sensing. *IEEE Photonics Journal* **2017,** *9* (3), 1-9.
38. Hashiyada, S.; Narushima, T.; Okamoto, H., Imaging chirality of optical fields near achiral metal nanostructures excited with linearly polarized light. *ACS Photonics* **2018,** *5* (4), 1486-1492.
39. Hashiyada, S.; Narushima, T.; Okamoto, H., Active control of chiral optical near fields on a single metal nanorod. *ACS Photonics* **2019,** *6* (3), 677-683.
40. Jackson, J. D., Classical electrodynamics. American Association of Physics Teachers: 1999.
41. Grosjean, T.; Mivelle, M.; Baida, F.; Burr, G.; Fischer, U., Diabolo nanoantenna for enhancing and confining the magnetic optical field. *Nano. Lett.* **2011,** *11* (3), 1009-1013.
42. Ögüt, B.; Vogelgesang, R.; Sigle, W.; Talebi, N.; Koch, C. T.; van Aken, P. A., Hybridized metal slit eigenmodes as an illustration of Babinet's principle. *ACS Nano* **2011,** *5* (8), 6701-6706.
43. Singh, A.; Calbris, G.; van Hulst, N. F., Vectorial Nanoscale Mapping of Optical Antenna Fields by Single Molecule Dipoles. *Nano. Lett.* **2014,** *14* (8), 4715-4723.
44. Degiron, A.; Lezec, H.; Yamamoto, N.; Ebbesen, T., Optical transmission properties of a single subwavelength aperture in a real metal. *Opt. Commun.* **2004,** *239* (1-3), 61-66.
45. Curto, A. G. Optical antennas control light emission. Universitat Politècnica de Catalunya, 2014.
46. Park, Y.; Kim, J.; Roh, Y.-G.; Park, Q.-H., Optical slot antennas and their applications to photonic devices. *Nanophotonics* **2018,** *7* (10), 1617-1636.
47. Solomon, M. L.; Abendroth, J. M.; Poulikakos, L. V.; Hu, J.; Dionne, J. A., Fluorescence-detected circular dichroism of a chiral molecular monolayer with dielectric metasurfaces. *J. Am. Chem. Soc.* **2020,** *142* (43), 18304-18309.
48. Punj, D.; Mivelle, M.; Moparthi, S. B.; van Zanten, T. S.; Rigneault, H.; van Hulst, N. F.; García-Parajó, M. F.; Wenger, J., A plasmonic/antenna-in-box/'platform for enhanced single-molecule analysis at micromolar concentrations. *Nat. Nanotechnol.* **2013,** 8, 512–516. https://doi.org/10.1038/nnano.2013.98
49. Leite, T. R.; Zschiedrich, L.; Kizilkaya, O.; McPeak, K. M., Resonant Plasmonic–Biomolecular Chiral Interactions in the Far-Ultraviolet: Enantiomeric Discrimination of sub-10 nm Amino Acid Films. *Nano. Lett.* **2022,** *22* (18), 7343-7350.

50. Hendry, E.; Carpy, T.; Johnston, J.; Popland, M.; Mikhaylovskiy, R.; Lapthorn, A.; Kelly, S.; Barron, L.; Gadegaard, N.; Kadodwala, M., Ultrasensitive detection and characterization of biomolecules using superchiral fields. *Nat. Nanotechnol.* **2010,** *5* (11), 783-787.
51. Alizadeh, M.; Reinhard, B. r. M., Plasmonically enhanced chiral optical fields and forces in achiral split ring resonators. *ACS Photonics* **2015,** *2* (3), 361-368.
52. Davis, T.; Hendry, E., Superchiral electromagnetic fields created by surface plasmons in nonchiral metallic nanostructures. *Phys. Rev. B* **2013,** *87* (8), 085405.
53. Neugebauer, M.; Banzer, P.; Nechayev, S., Emission of circularly polarized light by a linear dipole. *Science advances* **2019,** *5* (6), eaav7588. DOI: 10.1126/sciadv.aav7588